

Electron Transfer Activation of a Second Water Channel for Proton Transport in [FeFe]-Hydrogenase

Olaseni Sode and Gregory A. Voth^a

Department of Chemistry, James Franck Institute, Institute for Biophysical Dynamics, Computation Institute, The University of Chicago, Chicago, Illinois, 60637 and Computing, Environment & Life Sciences, Argonne National Laboratory, Argonne, Illinois, 60439

Hydrogenase enzymes are important because they can reversibly catalyze the production of molecular hydrogen. Proton pathways have been previously studied that involve residue Cys299 in a water channel leading to the active site of the enzyme. It has been shown recently that a separate water channel (WC2) is coupled with electron transport to the active-site of the [FeFe]-hydrogenase. The water-mediated proton transport mechanisms of the enzyme in different electronic states have therefore been studied using the multistate empirical valence bond (MS-EVB) reactive molecular dynamics method. In a single electronic state A^{2-} , a water wire was formed through which protons can be transported, with a low free energy barrier. The remaining the electronic states were shown, however, to be highly unfavorable to proton transport in WC2. A double amino acid substitution is predicted to obstruct the proton transport in electronic state A^{2-} mutation was made to electronic state A^{2-} by closing a cavity for water filling near the proximal Fe of the active-site.

I. INTRODUCTION

There has long been interest in understanding the family of biological redox enzymes known as hydrogenases.¹⁻⁶ One of the main reasons for this interest is the potential biomimetic functionality the enzymes present through their ability to reversibly catalyze the reduction of protons and the oxidation of molecular hydrogen, i.e.,



for the use as an energy source.⁷ The current alternatives for these processes are expensive and relatively

^a Author to whom correspondence should be addressed. Electronic mail: gavoth@uchicago.edu.

rare. The uncatalyzed cleavage of the dihydrogen bond is very difficult, requiring on the order of +100 kcal mol⁻¹ and the best synthetic catalyst for this redox reaction is the scarce platinum metal. The hydrogenase proteins, with base metals of iron and nickel, provide a possible framework to reduce the operational cost of the production and consumption of H₂.

The hydrogenase family is categorized by its transition metal components in the enzyme active-site. [NiFe]-, [FeFe]-, and [Fe]-only are the three main hydrogenase classes^{2,3,8,9} and only the [Fe]-only, or cluster free hydrogenase, does not catalyze the reduction of protons or the oxidation of molecular hydrogen. [NiFe] is used typically for hydrogen oxidation, while [FeFe] participates mostly in proton reduction, although bidirectional enzymes are also known. This is evidenced by the different catalytic rates.

Much research has been devoted to the hydrogenase catalytic cycle in both the [FeFe] and [NiFe] enzymes.^{2,10-12} The structure and spin state of the active-site have been extensively studied along with the reaction mechanism of the catalysis, especially in the nickel complex.^{11,13} Since the functionality of the hydrogenase enzymes are predicated on charge separation and/or association, many recent studies have also focused on the different pathways protons and electrons take.¹⁴⁻¹⁸ In particular, a recent study by McCullagh and Voth¹⁸ looked at the electron transport pathway in the [FeFe]-hydrogenase from the exterior of the protein to the enzyme active-site, where it was shown to be thermodynamically favorable. In a study by Shaw and coworkers,¹⁴ the proton transport pathways were explored, and it was found that the amino acids play a large role in transferring the excess proton through the protein. The present work builds upon these past studies in investigating the proton transport pathways of the [FeFe]-hydrogenase enzyme, especially via a second, electronic state-dependent water channel predicted to exist in Ref. ¹⁸.

The crystal structure of the [FeFe]-hydrogenase *Clostridium pasteurianum* (CpI) is shown in Fig.

1a.¹⁹⁻²¹ The protein is composed of four subdomains, of which the active-site subdomain is the largest. Within the active-site domain is located the eponymous metal center of the protein surrounded by over 300 amino acids and an Fe₄S₄ cuboid.²⁰ The di-iron cluster active-site and the cuboid make up what is referred to as the H-cluster. They are joined together by a cysteine ligand bridge (Fig 1b). The Fe atom in the di-iron cluster closer to the cuboid is termed the proximal iron and the other is termed the distal iron. In the active-site, each Fe atom is coordinated by both a CN and CO ligand. The di-iron atoms are bridged together by a dithiolate ligand typically assigned to be the di(thiomethyl)amine (DTMA),²¹ di(thiomethyl)ether²² or propanedithiolate²³ groups. Another CO ligand also bridges the two Fe atoms, but, depending on the redox state, it is also found to be bound to only the distal iron atom.¹¹ In the remaining subdomains, denoted as clusters A, B, and C, three more iron-sulfur cuboids are situated farther away from the active-site. Lastly, a Fe₂S₂ cluster is also found in the protein.

Nearly all of the studies which deal with proton transfer through the [FeFe]-hydrogenase protein into the enzyme active-site focus on the water channel (WC1) consisting of three different proton transfer pathways originating from the protein surface at the Glu282, Lys571 and Glu368 residues.¹⁴ All of these pathways include protonatable amino acids, are minimally water-based, and converge at the Cys299 residue near the active-site. Predicted mutations of Cys299, Glu279 and Glu282 to serine, alanine, leucine and aspartic acid were also shown to block or drastically hinder catalytic activity.^{14, 24} Recently, a second water channel (WC2) was found that was activated by electron transport to the active-site and that did not involve the Cys299 residue.¹⁸ Specifically, when cluster A is reduced (state A²⁻), a loop containing Gly418 and Ala419 separates from another loop containing Gly502 and Gly503, which allows water to fill this empty cavity. Understanding this newly predicted water channel, and the role it plays in the concerted proton and electron transfer in the [FeFe]-hydrogenase may be important to fully understanding the biomimetic functionality and potential of these enzymes. This is the focus of the

present paper.

In the present study, we use multistate empirical valence bond (MS-EVB) reactive MD simulations²⁵⁻²⁹ to investigate the proton transport process in WC2 of the [FeFe]-hydrogenase. Since the charge defect associated with the excess proton prefers to be delocalized across several molecular species, in particular water molecules, the protons are known to “hop” through water wires via the intermediate Zundel-like ($\text{H}_2\text{O}-\text{H}^+-\text{OH}_2$) structure. This is known as the Grotthuss mechanism.²⁷ The MS-EVB MD methodology allows for such dynamic alteration of the bonding topology during MD simulations, which can be used in general for any chemical reaction, but here is restricted to only proton transfer between water molecules. Proton transport pathways were found using MS-EVB combined with umbrella sampling and the free energy profiles were also characterized. Mutations in state A^{2-} were also engineered in silico to better understand the water-wire network and how the protein structure responds. The double mutations Gly418 to phenylalanine (G418F) and Gly502 to valine (G502V) were thus studied for state A^{2-} .

In the following section, the details of the atomistic MD simulation for electronic states A^{2-} , B^{2-} , and C^{2-} will be presented. The mutated state A^{2-} simulation setup will be described as well. Also in this section the method used to find proton hopping channels and to characterize their free energy surfaces is detailed. The subsequent discussion section is organized to first look at the proton transport pathways of the electronic states and then to elaborate on their free energy profiles. The mutant pathway and free energy profile were also explained here. Concluding remarks are then provided.

II. METHODOLOGY

A. Simulation Setup

The [FeFe]-hydrogenase protein, taken from the X-ray crystal structure of *Clostridium*

paseurianum (PDB code 1FEH),²⁰ and was used as the starting geometry for all simulations. The protein contains a total of 574 amino acid residues and six metal centers. The central metal center, the active-site of the protein, consists of a [2Fe]-subcluster to which carbonyl and cyanide groups are ligated. In this work, the bridging groups were taken to be a di-thiomethylamine (DTMA) and a carbonyl group. The active-site is covalently linked to a Fe₄S₄ cuboid metal center by a cysteine residue, while three other cuboid metal centers are present throughout the protein. The remaining metal center is of the chemical formula Fe₂S₂. The force field parameters for all standard amino acids were taken to be the CHARMM27 configurations with CMAP corrections.³⁰ For the Fe clusters and the corresponding amino acid ligands, the force field parameters were taken from the published results of Chang and Kim.³¹ The details of the parameter modifications done in the current work can be found in the Supporting Information of the published work by McCullagh and Voth.¹⁸

All of the initial configurations of the hydrogenases at varying electronic states were taken from snapshots of trajectories from the published results of McCullagh and Voth,¹⁸ where the proteins were simulated for at least 50 ns. The proteins were completely solvated by waters forming a rectangular simulation box, an additional proton was added to the bulk water near the active-site of the hydrogenase, and counter ions were added to neutralize the system charge. The systems were equilibrated again for 2 ns using a Langevin thermostat and barostat set to 300 K and 1.0 bar using the NAMD 2.8 software.³² The same protocol was used for the mutant simulation except that after the mutant residues were added to the snapshot along with the waters and ions of the A²⁻ electronic state, the protein was minimized using the conjugate gradient for 1000 steps. The system was then equilibrated for 50 ns with the NVT ensemble.

B. MS-EVB Modeling

The details of the MS-EVB methodology are described quite extensively in many places^{25-27, 29, 33}

and to provide a general introduction to the method, a brief description is included here. For more information about the force field, the reader is encouraged to look at the other publications on the topic. In the present work, the MS-EVB3.1 model, described in the Supporting Information of Ref. ³⁴, was used.

The MS-EVB model is a molecular mechanics scheme in which bond topologies are not fixed, thus allowing for chemical reactions, such as in this case proton transport, throughout the MD simulation. To do this, the bonding topologies, labeled by $|i\rangle$, represent diabatic states in the MS-EVB Hamiltonian, given by

$$H^{\text{EVB}}(\vec{r}) = \sum_{ij} |i\rangle h_{ij}(\vec{r}) \langle j| \quad (2)$$

where $h_{ij}(\vec{r})$ and \vec{r} represent the matrix elements and the nuclear degrees of freedom, respectively. The matrix is dynamically constructed from the dynamically selected diabatic states and diagonalized at each MD timestep. The off-diagonal elements of the MS-EVB Hamiltonian describe the coupling between the diabatic states and are parameterized to reproduce *ab initio* potential surfaces and experimental properties.

Also, in order to better describe the protonic charge defect of the excess proton, the center of excess charge (CEC) variable is used, given by

$$\vec{r}_{\text{CEC}} = \sum_i^{N_{\text{EVB}}} c_i^2(\vec{r}) \vec{r}_i^{\text{COC}} \quad (3)$$

where $c_i^2(\vec{r})$ is the contribution of diabatic state i to the ground state potential energy surface, N_{EVB} is the total number of diabatic states, and \vec{r}_i^{COC} is the center of charge vector, given by

$$r_i^{\text{COC}} = \frac{\sum_{k \in i} |q_k| \vec{r}_k}{\sum_{k \in i} |q_k|} \quad (4)$$

where q_k is the partial charge on the k th atom. In short, the center of charge, r_i^{COC} , can be thought to represent the position of the hydronium ion for the diabatic state i , while the CEC coordinate tracks the full excess proton charge defect, which can be delocalized by the Grotthuss mechanism. The MS-EVB simulations were performed using the Rapid Approach for Proton Transfer and Other Reactions (RAPTOR)^{27, 29} add-on package of the LAMMPS³⁵ MD code.

C. Free Energy Calculations

The free energy simulations were carried using the umbrella sampling (US)³⁶⁻³⁸ method. The umbrella windows were positioned at equidistant points along a straight line connecting the bulk water to the protein active-site. For each electronic state and the mutant, a US simulation was performed using cylindrical coordinates, where a force constant of $10 \text{ kcal mol}^{-1} \text{ \AA}^{-2}$ was applied in the axial direction and a smaller potential of $0.1 \text{ kcal mol}^{-1} \text{ \AA}^{-2}$ was applied in the perpendicular directions. As such, the excess proton CEC is very unhindered in the perpendicular direction and can explore any radial area. The initial US simulations were “path-finding” and even an arbitrary, curvilinear path can be identified. A separate US simulation was performed again for the calculations of the free energy again with cylindrical coordinates. The weighted histogram analysis method (WHAM)³⁶ was used to construct the potential of mean force (PMF) from the umbrella windows. The PMF is the free energy profile for the proton transport via both standard diffusion and Grotthuss shuttling.

III. RESULTS

A. Proton Pathways

In order to better understand the nature of the proton transport pathways in WC2, water density

maps were constructed from equilibration simulations at each electronic state of the [FeFe]-hydrogenase protein. These are shown in Fig. 2. The density in state A^{2-} (Fig. 2a) is the most pronounced, with large pockets of water in several locations in WC2. A water wire leading to the proximal Fe of the active-site is also present. In fact, a large pocket of water molecules is observed between Ser232 and Gly502. A clear contrast is observed in electronic state B^{2-} (Fig. 2b), where there is almost no water density within the water channel. A small pocket of water is located near Thr250 and Val249. In state C^{2-} , shown in Fig. 2c, this pocket has shifted closer to the active-site. Somewhat surprisingly there exists two other small regions of water density near the proximal Fe and FeS cuboid in state C^{2-} , which are obstructed from the active-site by Cys503 and Ser232. Lastly, Fig. 2d shows the water density map of the double mutant G418F/G502V in state A^{2-} . Similar to the wild type protein, many water molecules fill WC2; however, near the active site, the water wire is no longer observed. The same is true for the pocket near Ser232 and Gly502.

For each electronic state considered, an initial “path-finding” US simulation was performed to find a pathway for the excess proton CEC connecting the active-site to the bulk. Because comparisons were only made between pathways in different electronic states, the path-finding US method was deemed sufficient, as opposed to a more elaborate metadynamics-based approach.¹⁵ To this point, the pathways were not completely unbiased since some aspects of the paths were known *a priori*. In each simulation the hydrated proton (hydronium-like species) was started in bulk water. In each electronic state A^{2-} , B^{2-} and C^{2-} , the excess proton CEC was initially positioned near residues Thr250 and Gln533, about 20 Å away from the active-site. Here, the systems were equilibrated once again for an additional 50 ps at 300K. The umbrella windows were then evenly spaced in each of the different states, (40 windows for electronic state B and C and 30 windows for state A) along a straight line starting from the active-site to the initial hydronium position. Each of the path-finding US simulations consisted of 50 ps

of sampling at each umbrella window. The CEC originated in the bulk and was slowly sampled through the protein to the active-site.

In electronic state A^{2-} , shown in Fig. 3a, a curvilinear path was found that wraps mainly around Pro231, which is positioned directly under the 2[Fe]-subcluster of the active-site. This followed the water wire that was observed here. The blue spheres in Fig. 3 indicate the instantaneous excess proton CEC position during the simulation. Other residues, which allow for the presence of a water wire, include Ser232, Gly418, Gly502, Val504, and Cys503. This pathway was suggested in our previous computational work. At about 6 Å from the active-site and near the Ser232 residue, the water pathway becomes something of a branch point, where it connects to other nearby pathways, much in the same way the pathways in WC1 converge near the Cys299 residue. This underlines the importance of the residues in this region in allowing or disallowing proton transport to the active-site. It would appear that even if one pathway is blocked another can open up if this region was not properly restricted.

In electronic state C^{2-} , a pathway was found as shown in Fig. 3c. Here the hydronium is located near the loop residues, Asp248, Val249, and Thr250. After equilibration the excess proton CEC is sampled through a pocket of amino acids, including Arg234, Ala415, and Leu530, that block access to the active-site. The CEC changes direction once it passes Leu530, as a direct path to the H-cluster is obscured by the Pro231 and the large Phe417 residues near the distal Fe of the active-site. A very curvilinear path is taken to the distal side of the active-site by the CEC, where a small opening allows the CEC to approach the metal center. Unlike in electronic state A^{2-} , where a persistent water wire is found connecting the bulk water to the active-site, no such water wire was found for state C^{2-} , even after the initial US simulation. Thus, at times the hydrated proton structure was only solvated by one other water molecule as it maneuvered along the pathway.

The pathway exhibited by electronic state B^{2-} (Fig. 3b) is similar to that of state C^{2-} . Again the hydrated proton, initially positioned much farther away from the active-site than in electronic state A^{2-} near residue Asp248, moves through a pocket created by residues Arg234, Ala415, and Leu530 at about 10.5 Å away from the active-site. Unlike in state C^{2-} , there is more space in this region and the excess proton CEC can more easily move between these residues. This is also the case closer to the active-site. Whereas before in state C^{2-} the large phenylalanine and proline residues obscured the access of the CEC to the proximal Fe of the subcluster, here there is just enough space opened up for the CEC to directly access the active-site. As Fig. 3c shows, the pathway found is not nearly as curvilinear as it makes its way through the protein. As was previously the case, because of the restrictive nature of the path, no water wire exists along the determined path. Instead, only few water molecules and the excess proton are pulled through the obstructing residues.

In electronic state A^{2-} with mutations of residues G418F and G502V, a proton transport path was also found using the path-finding US simulations and the instantaneous CEC positions are shown in Fig. 3d. The hydrated proton was initially positioned about 18Å away from the active site, near Arg234. The mutations of the glycine residues near the 2[Fe]-subcluster obstruct the water wire from approaching the proximal Fe atom as was the case in state A^{2-} . This is mostly as a result of the large hydrophobic phenylalanine group but the valine residue also aids in preventing the water molecules from approaching the active site near the bridging Cys503 ligand. Preliminary equilibrations were done with only a single site mutation G418F and a water wire pathway similar to state A^{2-} was still present. However, the CEC instead travels on the opposite side of the Pro231 residue towards the distal Fe atom. There is no water wire seen on this case, but enough space for the CEC to squeeze through to the active site between the Asn269, Phe417, Pro231 and G418F residues.

Because in the current simulation the MS-EVB model does not allow for the protonation of

neighboring amino acids, it could be the case that the CEC might be more stabilized by such protonation events. However, because of the general restricted nature of the pathways in both state B and C, this does not seem very likely. The only protonatable amino acid along the water pathways is Asp248 and this is located near the mouth of the water channel in state B²⁻ and C²⁻. In electronic state A²⁻, where the initial excess proton CEC position is situated much closer to the active-site, the water wire is easily discernible and no protonatable residues are present.

B. Free Energy Profiles

Because the loops in electronic state B²⁻ and C²⁻ work to envelope the active-site, thus preventing water from approaching, the proton transport pathways in the different electronic states are noticeably different and this is reflected in the PMFs, all shown in Fig. 4. Fig. 4a shows the PMF (free energy profile) for proton transport in electronic state A²⁻. The initial portion of the PMF on the right side of Fig. 4a has the excess proton CEC at the mouth of WC2 from the bulk near the pocket created by Arg234, Leu530 and Asn236. This is shown as an initial small uphill climb in the free energy of nearly one kcal mol⁻¹ with a peak at 10 Å from the active-site. Beyond this initial characteristic, the main feature of this PMF is its minimum about 3 - 4 Å away from the center of mass of the active-site (X = 0 Å). It is important to note that the radius of the di-iron active site with its carbonyl and cyanide ligands is around 3 Å. Since no proton transfer was allowed in the present MS-EVB model between the excess proton on the water molecules and the di-iron complex as happens in the catalytic cycle, the CEC encounters the wall of the active-site. This is shown in the PMF of state A²⁻ as a sharp rise beginning at closer than 3 Å. As the CEC bends its way around Pro231, the free energy slowly decreases until it reaches 7 Å from the active-site. In this region a small pocket is created by Ser232, Val504, and Ile522, after which the free energy experiences a much more steep decrease until the minimum is reached.

The reason for the relatively small free energy barrier in the PMF of electronic state A^{2-} is a direct result of the unbroken water wire leading from the bulk to the active-site. It was shown previously¹⁸ that the electrostatic potential (ESP) along WC2 became more negative as a function of the inverse distance to the active site. This attractive ESP not only allows for the presence of the existing water wire through the separation of two loops, but it also adds an attractive force which drives the excess proton CEC towards the active-site of the enzyme. Once the CEC is past the pocket near the positively charged Arg234, its free energy is completely exergonic until it reaches the H-cluster.

The PMFs of state B^{2-} and C^{2-} , shown in Fig. 4b and 4c respectively, are similar to each other, yet have some distinguishable feature. The main characteristic of both of the PMFs is their nearly continuous uphill nature from the bulk situated near Gln533 and Asp248 (located at $X = 16 \text{ \AA}$) to the metal center (near $X = 2 \text{ \AA}$). However, the two surfaces are not identical. To start, the PMF in electronic state C^{2-} experiences a much steeper rise as the hydrated CEC approaches the enzyme center. Also there are almost no plateau regions except for when the CEC is positioned about $X = 13 \text{ \AA}$ away from the active site. This corresponds with the water pocket shown in Fig. 2b, formed by Leu530, Arg234 and Val249. In state A^{2-} , this pocket opens up and includes water molecules from the bulk. The same plateau region is observed in state B^{2-} but is more pronounced. This agrees with what we would expect given the presence of more water molecules in the Arg234, Ala415, and Leu530 pocket in state B^{2-} . Also, unlike in state C^{2-} where the CEC experiences relatively easy access to the pocket near Arg234, in the reduced cluster B state access to this pocket is very much constrained by Asp248, Val249, Thr250, and Gln533, resulting in a steep rise at the right edge of the PMF. This rise could be slightly mitigated by the protonatable aspartic acid residue, but the general trend still stands. As the CEC moves closer to the H-cluster from the pocket, the PMF surface again rises quickly in both states. In state B^{2-} this free energy rise is the result of the CEC moving through the arginine and proline residues by the active site until it

levels off in the water pocket near Arg234 at about 9 Å. The PMF of state C^{2-} rises continuously only as it passes through Thr250 and Gln533. It is at this point in the CEC pathways of states B^{2-} and C^{2-} that the pathways diverge. As the CEC in the reduced cluster B state follows Pro231 and Ser232 towards the proximal Fe of the active-site, the PMF increases steadily. This is in direct contrast to state A^{2-} , which follows the same pathway but experiences a decrease in free energy. The free energy of state C^{2-} also increases as the CEC approaches the active-site, this time from the distal Fe atom. Again, the increase is steady until about 6 Å, after which the free energy rises much more. However, it is clear overall that the pathway taken by the hydrated proton CEC in electronic states B^{2-} and C^{2-} is unfavorable in either case, especially compared to the free energy profile in electronic state A^{2-} .

The above results suggest a special role for WC2 when the enzyme is in the A^{2-} state, i.e., an electron transfer activated proton transport pathway. In order to explore this behavior and to make an experimentally testable prediction, the proton transport PMF was calculated for electronic state A^{2-} with the double mutation G418F and G502V. The result is shown as the dashed line in Fig. 4a. The most noticeable feature is that the transporting the CEC towards the active-site is no longer exergonic. Instead, the free energy becomes quite unfavorable. The free energy rises about 20-25 kcal mol⁻¹ above what was observed for A^{2-} state of the wild type enzyme. This results suggests that the G418F/G502V double mutant will significantly affect the proton transport behavior of the enzyme and likely its catalytic production of molecular hydrogen. (Unless, of course, the enzyme has robust “self-rescue” capabilities for proton transport pathways that we have not tested here.)

IV. CONCLUSIONS

The MS-EVB reactive molecular dynamics simulations were used along with free energy sampling to investigate the proton transport process in a second water channel (WC2) of [FeFe]-

hydrogenase. The proton transport in WC2 was explored in three different electronic states, as well as in the state A^{2-} with the double mutation G418F/G502V, to show how the excess proton CEC is able to access the enzyme active-site (or not). The path shown for electronic state A^{2-} without mutations, which curves around the Pro231 leading to the proximal Fe of the active-site, was the only path where a water wire exists throughout the simulations. A stable pocket was formed by Arg234, Ala235, Ala419, Ala415, and Ile416, which allowed water molecules to fill this area, below the Pro231 residue. In the other electronic states, this cavity was no longer present. The Arg234 residue obstructs any waters from filling this area, along with the coming together of a loop containing Asp248, Val248, and Thr250 with another loop containing Asn532, Gln533, and Asp534. The excess proton CEC was positioned initially farther away from the active site, which is hindered to the di-iron cluster and two separate pathways were taken by the electronic state B^{2-} and C^{2-} . The double mutant proton transport pathway was similar to the one taken by electronic state C^{2-} in which the CEC approached the distal Fe atom from the water pocket located by Arg234.

The free energy surfaces (PMFs) were also explored qualitatively with the US method for the three electronic states. It seems clear that the electronic state of the enzyme plays a large role in the ability of protons to move to and from the active-site in WC2. The pathway taken in state A^{2-} was the energetically favorable path, which agrees well with previous assumptions about WC2.¹⁸ The electronic states B^{2-} and C^{2-} show much more steep PMFs which are strongly uphill in nature. When the two glycine residues in WC2 were mutated (G418F/G502V), the proton transport PMF of state A^{2-} more closely resembled that of the other two states with an uphill free energy profile to the active site.

Although, the current work expands our understanding of the possible electronic state-dependent (activated) proton transport through WC2, there still exist many possibilities to further study in this area. For instance, a more thorough examination of the different proton pathways taken in WC2 could be

useful, including the relative energy differences associated with the excess proton CEC approaching the proximal or distal Fe of the active-site. Such results, in turn, would be tied to how the different catalytic cycles of the active-site either facilitate or hinder proton transport in both WC1 and WC2.

ACKNOWLEDGMENTS

The authors acknowledge the University of Chicago Research Computing Center and the Extreme Science and Engineering Discovery Environment (XSEDE) for computation resources. This research was supported by the (U.S.) Department of Energy (DOE) under Contract No. DE-AC02-06CH11357.

FIGURES

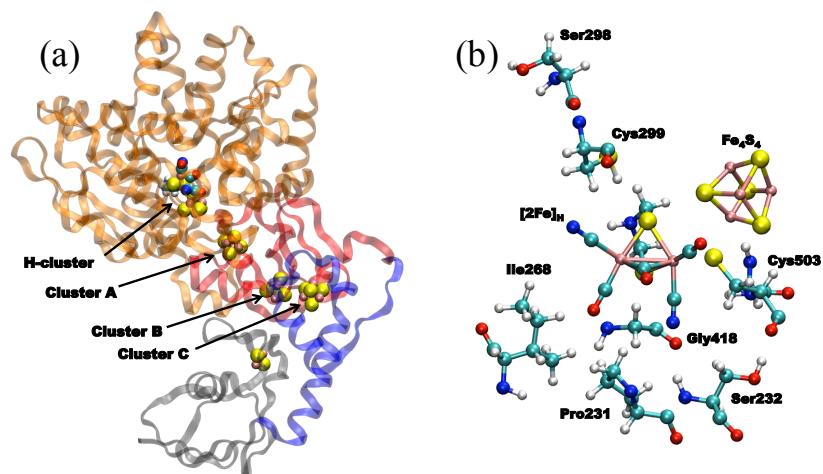


Figure 1. (a) [FeFe]-hydrogenase (PDB 1FEH) with the FeS metal centers shown in the VDW model. The active-site domain is colored orange, whereas the other three domains are shown in red, blue and gray. (b) The H-cluster, containing the FeS cuboid and Fe—Fe active-site, is shown along with nearby amino acid residues.

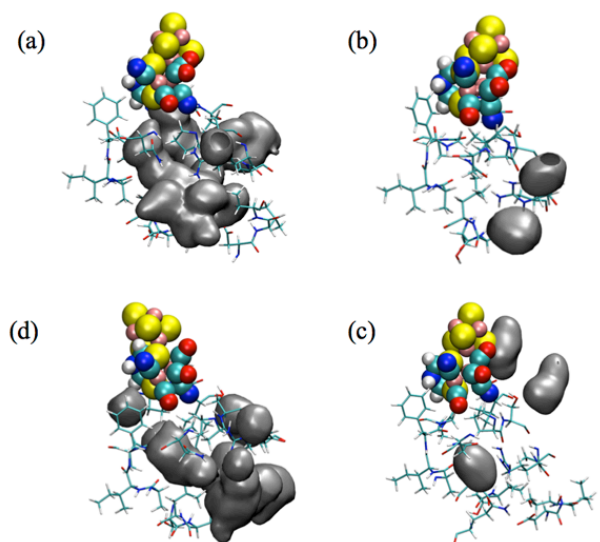


Figure 2. The water density maps of WC2 in electronic state A^{2-} (a), B^{2-} (b), C^{2-} (c), mutant (d) are shown (gray). Several residues are displayed along the water pathway as well as the H-cluster at the top of the figures.

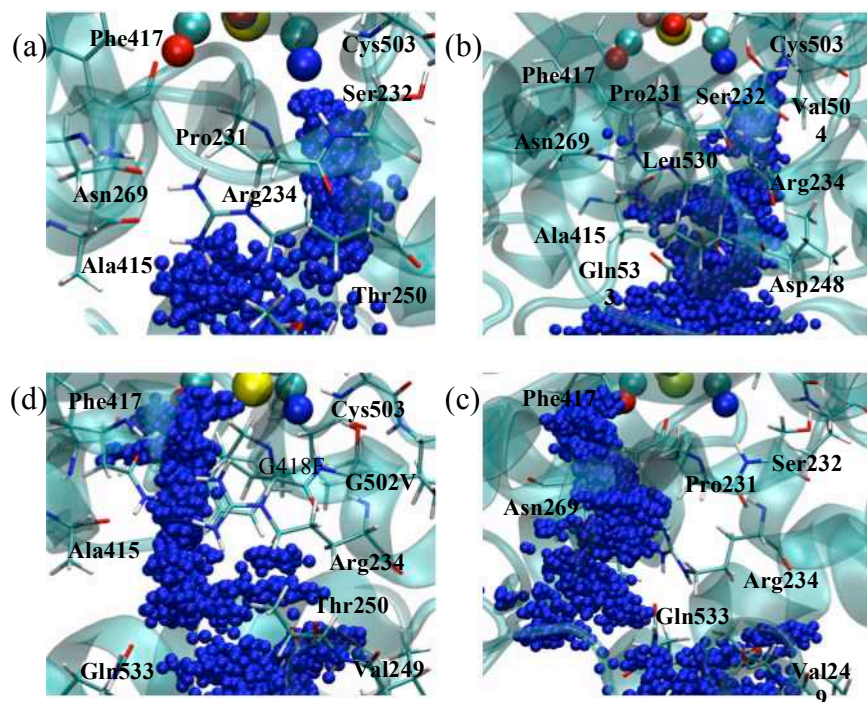


Figure 3. The WC2 pathways are shown in state A^{2-} (a), B^{2-} (b), C^{2-} (c), and the mutant (d) with several residues labeled. The blue spheres that constitute the pathway represent dynamical positions of the excess proton CEC. Several important residues are shown and labeled. The active-site is shown at the top of the figures and the protein exterior is located at the bottom.

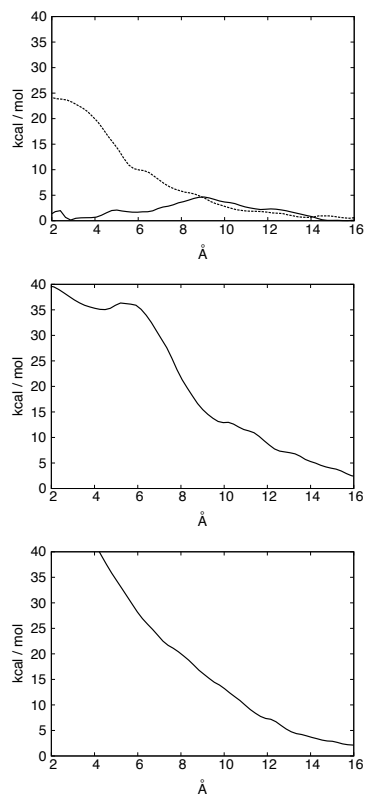


Figure 4. The FES of electronic states A^{2-} (a), B^{2-} (b), C^{2-} (c) are shown. The FES of electronic state A^{2-} with mutate residues is shown as a dashed line in (a). The x -axis is the reaction coordinate that leads from the enzyme exterior (right) to the enzyme interior (left). Note the differences in x -axis scale between the figures. The average bin errors are \pm kcal mol⁻¹.

This work was supported by the U. S. Department of Energy, Office of Science, under Contract No. DE-AC02-06CH11357.

VII. REFERENCES

1. J. C. Fontecilla-Camps, A. Volbeda, C. Cavazza and Y. Nicolet, *Chem. Rev.* **107**, 4273-4303 (2013).
2. W. Lubitz, H. Ogata, O. Rüdiger and E. Reijerse, *Chem. Rev.* **114**, 4081-4148 (2014).
3. M. Frey, *ChemBioChem* **3**, 153-160 (2002).
4. P. M. Vignais and B. Billoud, *Chem. Rev.* **107**, 4206-4272 (2007).
5. P. M. Vignais, B. Billoud and J. Meyer, *FEMS Microbiology Reviews* **25**, 455-501 (2001).
6. M. Wang, L. Chen, X. Li and L. Sun, *Dalton Trans.* **40**, 12793 (2011).
7. W. Lubitz, E. J. Reijerse and J. Messinger, *Energy Environ. Sci.* **1**, 15 (2008).
8. M. W. W. Adams, *Biochim. Biophys. Acta, Bioenerg.* **1020**, 115-145 (1990).
9. A. Volbeda, M.-H. Charon, C. Piras, E. C. Hatchikian, M. Frey and J. C. Fontecilla-Camps, *Nature* **373**, 580-587 (1995).
10. C. H. Chang, *J. Phys. Chem. A* **115**, 8691-8704 (2011).
11. P. E. M. Siegbahn, J. W. Tye and M. B. Hall, *Chem. Rev.* **107**, 4414-4435 (2007).
12. O. Gutiérrez-Sanz, M. C. Marques, C. S. A. Baltazar, V. M. Fernandez, C. M. Soares, I. A. C. Pereira and A. L. Lacey, *J Biol Inorg Chem* **18**, 419-427 (2013).
13. J. M. Keith and M. B. Hall, *Inorg. Chem.* **49**, 6378-6380 (2010).
14. B. Ginovska-Pangovska, M.-H. Ho, J. C. Linehan, Y. Cheng, M. Dupuis, S. Raugei and W. J. Shaw, *Biochim Biophys Acta* (2013).
15. I. Sumner and G. A. Voth, *J. Phys. Chem. B* **116**, 2917-2926 (2012).
16. V. H. Teixeira, A. M. Baptista and C. M. Soares, *Biophys. J.* **91**, 2035-2045 (2006).
17. V. H. Teixeira, C. M. Soares and A. M. Baptista, *Proteins* **70**, 1010-1022 (2007).
18. M. McCullagh and G. A. Voth, *J. Phys. Chem. B* **117**, 4062-4071 (2013).
19. Y. Nicolet, C. Piras, P. Legrand, C. E. Hatchikian and J. C. Fontecilla-Camps, *Structure* **7**, 13-23.
20. J. W. Peters, W. N. Lanzilotta, B. J. Lemon and L. C. Seefeldt, *Science* **282**, 1853-1858 (1998).
21. Y. Nicolet, A. L. de Lacey, X. Vernède, V. M. Fernandez, E. C. Hatchikian and J. C. Fontecilla-Camps, *J. Am. Chem. Soc.* **123**, 1596-1601 (2001).

22. A. S. Pandey, T. V. Harris, L. J. Giles, J. W. Peters and R. K. Szilagy, *J. Am. Chem. Soc.* **130**, 4533-4540 (2008).
23. Y. Nicolet, B. J. Lemon, J. C. Fontecilla-Camps and J. W. Peters, *Trends in Biochemical Sciences* **25**, 138-143.
24. A. J. Cornish, K. Gartner, H. Yang, J. W. Peters and E. L. Hegg, *Journal of Biological Chemistry* **286**, 38341-38347 (2011).
25. U. W. Schmitt and G. A. Voth, *J. Phys. Chem. B* **102**, 5547-5551 (1998).
26. U. W. Schmitt and G. A. Voth, *J. Chem. Phys.* **111**, 9361-9381 (1999).
27. J. M. J. Swanson, C. M. Maupin, H. Chen, M. K. Petersen, J. Xu, Y. Wu and G. A. Voth, *J. Phys. Chem. B* **111**, 4300-4314 (2007).
28. Y. Wu, H. Chen, F. Wang, F. Paesani and G. A. Voth, *J. Phys. Chem. B* **112**, 467-482 (2008).
29. T. Yamashita, Y. Peng, C. Knight and G. A. Voth, *J. Chem. Theory Comput.* **8**, 4863-4875 (2012).
30. A. D. Mackerell, D. Bashford, M. Bellott, R. L. Dunbrack, J. D. Evanseck, M. J. Field, S. Fischer, J. Gao, H. Guo, S. Ha, D. Joseph-McCarthy, L. Kuchnir, K. Kuczera, F. T. K. Lau, C. Mattos, S. Michnick, T. Ngo, D. T. Nguyen, B. Prodhom, W. E. Reiher, B. Roux, M. Schlenkrich, J. C. Smith, R. Stote, J. Straub, M. Watanabe, J. Wiórkiewicz-Kuczera, D. Yin and M. Karplus, *J. Phys. Chem. B* **102**, 3586-3616 (1998).
31. C. H. Chang and K. Kim, *J. Chem. Theory Comput.* **5**, 1137-1145 (2009).
32. J. C. Phillips, R. Braun, W. Wang, J. Gumbart, E. Tajkhorshid, E. Villa, C. Chipot, R. D. Skeel, L. Kalé and K. Schulten, *J. Comput. Chem.* **26**, 1781-1802 (2005).
33. T. J. F. Day, A. V. Soudackov, M. Čuma, U. W. Schmitt and G. A. Voth, *J. Chem. Phys.* **117**, 5839-5849 (2002).
34. J. G. Nelson, Y. Peng, D. W. Silverstein and J. M. J. Swanson, *J. Chem. Theory Comput.* **10**, 2729-2737 (2014).
35. S. Plimpton, *Journal of Computational Physics* **117**, 1-19 (1995).
36. S. Kumar, J. M. Rosenberg, D. Bouzida, R. H. Swendsen and P. A. Kollman, *J. Comput. Chem.* **13**, 1011-1021 (1992).
37. M. Souaille and B. t. Roux, *Comput. Phys. Commun.* **135**, 40-57 (2001).

38. L. Maragliano, A. Fischer, E. Vanden-Eijnden and G. Ciccotti, *J. Chem. Phys.* **125**, 024106 (2006).

The submitted manuscript has been created by UChicago Argonne, LLC, operator of Argonne National Laboratory ("Argonne"). Argonne, a U.S. Department of Energy Office of Science laboratory, is operated under Contract No. DE-AC02-06CH11357. The U.S. Government retains for itself, and others acting on its behalf, a paid-up nonexclusive, irrevocable worldwide license in said article to reproduce, prepare derivative works, distribute copies to the public, and perform publicly and display publicly, by or on behalf of the Government.